



**HAL**  
open science

## **Self-organization as a mechanism of resilience in dryland ecosystems**

Sonia Kéfi, Alexandre Génin, Angeles Garcia-Mayor, Emilio Guirado, Juliano Cabral, Miguel Berdugo, Josquin Guerber, Ricard Solé, Fernando Maestre

► **To cite this version:**

Sonia Kéfi, Alexandre Génin, Angeles Garcia-Mayor, Emilio Guirado, Juliano Cabral, et al.. Self-organization as a mechanism of resilience in dryland ecosystems. *Proceedings of the National Academy of Sciences of the United States of America*, 2024, 121 (6), pp.e2305153121. <10.1073/pnas.2305153121>. <hal-04547915>

**HAL Id: hal-04547915**

**<https://hal.umontpellier.fr/hal-04547915v1>**

Submitted on 16 Apr 2024

**HAL** is a multi-disciplinary open access archive for the deposit and dissemination of scientific research documents, whether they are published or not. The documents may come from teaching and research institutions in France or abroad, or from public or private research centers.

L'archive ouverte pluridisciplinaire **HAL**, est destinée au dépôt et à la diffusion de documents scientifiques de niveau recherche, publiés ou non, émanant des établissements d'enseignement et de recherche français ou étrangers, des laboratoires publics ou privés.



HAL Authorization

# 1 2 **Self-organization as a mechanism of resilience in dryland** 3 **ecosystems** 4

5 Sonia Kéfi<sup>1,2,5\*</sup>, Alexandre Génin<sup>1,3,11</sup>, Angeles Garcia-Mayor<sup>3,6</sup>, Emilio Guirado<sup>4</sup>,  
6 Juliano S. Cabral<sup>5,10</sup>, Miguel Berdugo<sup>6</sup>, Josquin Guerber<sup>1,12</sup>, Ricard Solé<sup>2,7,8</sup>,  
7 Fernando T. Maestre<sup>4,9</sup>  
8

9 <sup>1</sup> ISEM, CNRS, Univ. Montpellier, IRD, EPHE, Montpellier, France

10 <sup>2</sup> Santa Fe Institute, 1399 Hyde Park Road, Santa Fe, NM 87501, USA

11 <sup>3</sup> Utrecht University, Environmental Sciences, Copernicus Institute of Sustainable Development,  
12 Postbus 80.115, 3508TC Utrecht, the Netherlands

13 <sup>4</sup> Instituto Multidisciplinar para el Estudio del Medio “Ramón Margalef,” Universidad de Alicante,  
14 03690 San Vicente del Raspeig Alicante, Spain

15 <sup>5</sup> Ecosystem Modeling Group, Center for Computational and Theoretical Biology, University of  
16 Würzburg, Würzburg, Germany

17 <sup>6</sup> Department of Biodiversity, Ecology and Evolution, Faculty of Biology, Complutense University  
18 of Madrid, Madrid 28040, Spain

19 <sup>7</sup> Catalan Institution for Research and Advanced Studies-Complex Systems Lab, Universitat  
20 Pompeu Fabra, Barcelona 08003, Spain

21 <sup>8</sup> Institut de Biologia Evolutiva (CSIC-UPF), 08003 Barcelona, Spain

22 <sup>9</sup> Departamento de Ecología, Universidad de Alicante, Carretera de San Vicente del Raspeig s/n,  
23 03690 San Vicente del Raspeig, Alicante, Spain.

24 <sup>10</sup> School of Biosciences, College of Life and Environmental Sciences, University of Birmingham,  
25 B15 2TT Birmingham, UK.

26 <sup>11</sup> Estación Costera de Investigaciones Marinas, Pontificia Universidad Católica de Chile, Las  
27 Cruces 2690000, Chile

28 <sup>12</sup> Centre d'Ecologie et des Sciences de la Conservation (CESCO), MNHN, CNRS, Sorbonne  
29 Univ., 75005 Paris, France  
30

31 \* Corresponding author: Sonia Kéfi

32 Email: [sonia.kefi@umontpellier.fr](mailto:sonia.kefi@umontpellier.fr)  
33

34 **Author Contributions:** Conceptualization: SK, AG; Methodology: SK, AG; Investigation:  
35 SK, AG, EG, MB, JG; Visualization: SK, AG, EG, RS; Funding acquisition: SK, FTM;  
36 Supervision: SK; Writing – original draft: SK; Writing – review & editing: SK, AG,  
37 AGM, EG, JSC, MB, JG, RS, FTM

38 **Competing Interest Statement:** Authors declare that they have no competing interests.

39 **Classification:** major: Biological sciences; minor: Ecology

40 **Keywords:** drylands, self-organization, spatial patterns, desertification

41 **This PDF file includes:**

42 Main Text

43 Figures 1 to 5  
44  
45  
46  
47  
48  
49  
50

51  
52  
53  
54  
55  
56  
57  
58  
59  
60  
61  
62  
63  
64  
65  
66  
67  
68  
69  
70

**Abstract**

Self-organized spatial patterns are a common feature of complex systems, ranging from microbial communities to mussel beds and drylands. While the theoretical implications of these patterns for ecosystem-level processes, such as functioning and resilience, have been extensively studied, empirical evidence remains scarce. To address this gap, we analyzed global drylands along an aridity gradient using remote sensing, field data and modeling. We found that the spatial structure of the vegetation strengthens as aridity increases, which is associated with the maintenance of a high level of soil multifunctionality, even as aridity levels rise up to a certain threshold. The combination of these results with those of two individual-based models indicate that self-organized vegetation patterns not only form in response to stressful environmental conditions but also provide drylands with the ability to adapt to changing conditions while maintaining their functioning, an adaptive capacity which is lost in degraded ecosystems. Self-organization thereby plays a vital role in enhancing the resilience of drylands. Overall, our findings contribute to a deeper understanding of the relationship between spatial vegetation patterns and dryland resilience. They also represent a significant step forward in the development of indicators for ecosystem resilience, which are critical tools for managing and preserving these valuable ecosystems in a warmer and more arid world.

71 **Significance Statement**

72  
73  
74  
75  
76  
77  
78  
79  
80  
81  
82

The spatial structure of vegetation in dryland ecosystems has long fascinated scientists due to its striking appearance. Through a combination of global field surveys, mathematical models, and remote sensing, we show that the mechanisms responsible for these patterns enable healthy dryland ecosystems to adapt to changing environmental conditions, including water shortages, by adjusting their spatial structure. Conversely, degraded ecosystems do not have this ability. Our findings underscore the critical role of spatial pattern formation in promoting resilience in dryland ecosystems. Moreover, these spatial patterns could serve as valuable indicators of ecosystem health under a changing climate, opening important perspectives for future research in this field.

83 **Main Text**

84

85 **Introduction**

86

87 Abrupt, irreversible changes in ecosystems are a serious concern given the forecasts for future  
88 environmental changes and their expected pace (1). Urgently needed tools are being developed to  
89 characterize and anticipate shifts in ecosystem functioning and stability. While many of these tools  
90 rely on analyzing temporal changes in ecosystem properties, the spatial structure of some  
91 ecosystems can also teach us about the way these ecosystems cope with stressors such as  
92 changes in climate (2–5). Indeed, interactions between species and their environment can generate  
93 emergent spatial patterns even in the absence of underlying heterogeneity, referred to as ‘self-  
94 organized’ patterns (3, 6, 7). Drylands are one of the textbook examples of ecosystems showing  
95 such patterns, as their vegetation cover presents a striking spatial structure that displays well-  
96 defined statistical properties across large spatial scales (2, 8–10). One of the most commonly  
97 hypothesized underlying mechanisms is that, in the harsh environmental conditions of drylands,  
98 established vegetation improves the local environmental conditions and alters the redistribution of  
99 resources – in particular water – from bare areas to vegetation patches, which promotes the spatial  
100 aggregation of plants (3, 7, 8, 11–14).

101

102 Theoretical studies have long suggested that self-organized spatial patterns could increase overall  
103 ecosystem function and resilience (3, 4, 6, 11, 13). Indeed, the capacity of drylands to spatially self-  
104 organize is predicted to allow them to maintain a higher productivity than what would be expected  
105 in the absence of spatial structure (3, 7, 11, 13). These self-organized patterns may change with  
106 environmental conditions, such as water shortage, giving drylands the ability to adapt and maintain  
107 productivity by adjusting their spatial structure (3, 11, 13). This is expected to lead to relatively  
108 stable levels of ecosystem functioning despite increasing stress, allowed by changes in spatial  
109 patterns. However, empirical support for this hypothesis is still elusive. Furthermore, spatial  
110 vegetation patterns can also hold the key to another generic phenomenon of interest: critical  
111 slowing down (5). Indeed, theoretical models have shown that self-organized spatial patterns could  
112 also be used as indicators of resilience loss because they reflect the speed required by the system  
113 to recover from perturbations (15): as a dynamical system approaches a point at which its stability  
114 changes drastically, it takes a longer time to recover from small perturbations, which leaves traces  
115 both in the temporal and in the spatial dynamics of the system (15, 16). As a consequence, spatial  
116 structure is expected to show increasing variance and auto-correlation (referred to as ‘spatial early  
117 warnings’) as the ecosystem loses resilience (meaning as its recovery capacity decreases) (5, 17).

118

119 Previous empirical studies have analyzed changes in vegetation patterns along local gradients (2,  
120 18, 19) or in specific aspects of the vegetation patches across large spatial scales (9, 10, 20).  
121 However, building a robust predictive framework for dryland ecosystems requires going a step  
122 further by confronting theoretical predictions from mechanistic models to empirical observations  
123 covering large geographical scales and stress gradients. Doing so is essential to validate with  
124 confidence the causality of theoretical predictions about vegetation spatial patterns, their  
125 importance in maintaining dryland ecosystem resilience, and to evaluate whether and how spatial  
126 patterns can be used as early warning signals for the onset of desertification and abrupt ecosystem  
127 shifts (2–5, 11).

128

129 Here, we provide novel empirical support for the hypothesis that changes in the spatial structure of  
130 vegetation lead to relatively stable levels of dryland ecosystem functioning despite increasing  
131 stress. We used a global data set of 115 dryland sites (Fig. 1), for which field and remotely-sensed  
132 data about their soil and vegetation features were gathered (21). After classifying the high  
133 resolution remote sensing images of our data set into presence/absence of vegetation, we  
134 estimated vegetation cover and quantified its spatial structure using relevant spatial metrics based  
135 on theoretical studies (5): patch-based metrics (number and size of the vegetation patches),  
136 hydrological connectivity (connectivity of the bare-soil area reflecting the overall potential of the  
137 landscape to redistribute or lose resources by runoff), and spatial early warnings (quantifying the  
138 resilience of the ecosystem) (see Materials and Methods). At the global scales, we directly

139 compared the observed trends in these metrics along an aridity gradient to those produced by two  
140 different theoretical models previously used to investigate the emergence of spatial patterns in  
141 drylands (8, 13). These models describe the spatio-temporal dynamics of the vegetation assuming  
142 local facilitation (i.e., plants improve their local environment thereby facilitating the recruitment of  
143 others in their direct neighborhood) and global competition for limiting resources such as water (see  
144 Materials and Methods).

## 145 146 **Results**

147  
148 A two-dimensional clustering analysis of the vegetation cover and soil multifunctionality (i.e., an  
149 index derived from field measurements of carbon, nitrogen and phosphorus in the soil) of the field  
150 sites surveyed revealed that our dryland sites could be split into two distinct groups of relatively  
151 'healthier' (those with relatively high cover and soil multifunctionality) vs 'degraded' sites (those with  
152 relatively low cover and soil multifunctionality; Figs. 2 and S11). These two groups of sites differ  
153 significantly in all spatial metrics measured on vegetation cover but spatial auto-correlation (i.e.,  
154 *Spectral Density Ratio*; Fig. 3). Compared to degraded sites, healthier sites have larger patches,  
155 less connected bare areas (i.e., lower *flowlength*) and an overall less fragmented vegetation cover  
156 (i.e., steeper slope of the patch size distribution) (Figs. 3 and 4).

157  
158 Across all the sites surveyed, the fragmentation of the vegetation cover increases with aridity,  
159 driving changes in patch-based metrics that match the expectation from theoretical models (Figs.  
160 5 A, B and S7 in SI D). As environmental conditions become more stressful, the loss and  
161 fragmentation of vegetation cover led to a change in the shape of the patch size distribution (2, 22,  
162 23) and to an increase in the connectivity of bare-soil areas, as shown by increased values of  
163 *flowlength* (24). These trends need to be compared to the expected changes caused by the loss of  
164 vegetation cover for random spatial structure, hereafter called null model (see Material & Methods),  
165 to assess whether the observed changes can be purely explained by a decrease in cover under  
166 more arid conditions. We found that the observed breakdown of the patch size distribution in field  
167 sites is weaker than expected in the null model (compare the colored and the grey points for patch-  
168 based metrics in Figs. 5 A, B and S7). This means that vegetation in drylands is more spatially-  
169 structured than expected and is growingly so as aridity increases.

170  
171 Separate analyses of healthier and degraded sites revealed that the relative increase in spatial  
172 structure with aridity mainly occurs for the healthier sites (Fig. 5 C left). These results indicate that  
173 healthier sites thereby keep adapting their spatial structure as environmental conditions worsen.  
174 For all patch-based metrics evaluated, the deviation from randomness increases with aridity. This  
175 result suggests an increasing role of mechanisms enhancing the spatial aggregation of plants along  
176 the aridity gradient (8) (Fig. S8, S9). Indeed, in the absence of such processes, spatial structure  
177 emerges in the two theoretical models but is not different from a null expectation (Fig. S8,  
178 S9). Possible underlying mechanisms to explain our results include positive plant interactions (7),  
179 eco-hydrological feedbacks driving resource (especially water) redistribution in the landscape (24,  
180 25), exogenous phenomena (e.g., spatial structure in soil moisture (26)), or a combination of these  
181 mechanisms. The nature of our survey and analyses does not allow us to strictly conclude on the  
182 presence and importance of such mechanisms. However, the fact that bare-soil connectivity  
183 increases with aridity in the healthier group of sites - as shown by a significant increase in *flowlength*  
184 - and the fact that it does so more than in the null model (Fig. 5 C left), suggests that at least water  
185 distribution within the ecosystem plays a role (25). Indeed, an increase in *flowlength* means that  
186 vegetation patches receive resources (e.g., water, nutrients) from a larger bare-soil area than would  
187 be expected with a randomized spatial structure.

188  
189 In the degraded sites, trends in patch-based and in hydrological connectivity metrics break down  
190 along the aridity gradient: all trends are weaker than those in the healthier group of sites – several  
191 being not significant -, and they are closer to the null expectation (Fig. 5 C right). These findings  
192 indicate that the ability of the sites to undergo spatial reorganization under stress diminishes,  
193 associated with a decline in functioning. This is evident from the significant decrease in soil

194 multifunctionality observed for these sites in response to increasing aridity ( $p=1.2 \cdot 10^{-5}$ , Fig. S13 in  
195 SI).

196  
197 For the healthier sites, since only spatial variance changes significantly but not spatial  
198 autocorrelation, the spatial early warnings suggest no sign of resilience loss as aridity increases  
199 (Fig. 5 C left). This is consistent with those sites showing limited signs of 'suffering' from increasing  
200 aridity: cover decreases significantly with aridity because of constraints in water availability ( $p=3.7$   
201  $10^{-7}$ , Fig. S13 in SI), but functioning is maintained through the spatial reorganization of the cover  
202 (no significant decrease in soil multifunctionality with aridity;  $p=0.8$ , Fig. S13 in SI). However, in the  
203 degraded group of sites, spatial early warnings do suggest a loss of resilience as aridity increases  
204 (Fig. 5 C right), which probably reflects an overall physiological threshold of the vegetation at the  
205 end of the aridity gradient (27).

## 206 207 208 **Discussion**

209  
210 Our results, using a thorough evaluation of multiple spatial metrics – which reflect different facets  
211 of ecosystem resilience – provide novel insights on how drylands cope with abiotic stress and how  
212 their spatial structure contributes to improve their resilience to increased aridity conditions. Despite  
213 the large environmental variability found across the different field sites studied, the overall  
214 consistency of the observed changes in spatial metrics along an aridity gradient with theoretical  
215 predictions is remarkable.

216  
217 In this work, we have considered two different minimal models of dryland dynamics that share local  
218 facilitation and non-local (long-range) effects as the two necessary drivers that generate self-  
219 organized patterns with fat-tailed cluster distributions. Despite their differences, [these two models](#)  
220 successfully matched the repertoire of [spatial patterns found in our data](#) (2, 8, 22). This supports  
221 the idea of universality as defined in physics: macroscopic patterns in far-from-equilibrium systems  
222 can be accounted for from minimal interaction rules (28–30). [In other words, simple mechanistic](#)  
223 [models can provide reliable predictions beyond the specific, low-scale details. It is noteworthy that](#)  
224 [other types of drylands than the ones studied here](#), such as semiarid savannas, [have been found](#)  
225 [to exhibit a different type of behavior: available data](#) (31) and a different class of stochastic models  
226 (26) indicate that their spatial patterns [show broadly-similar features as those found in our data but](#)  
227 [are](#) caused by exogenous phenomena associated with the formation of soil moisture islands that  
228 determine the spatiotemporal dynamics of tree clusters (26). [In these latter systems, we do not](#)  
229 [expect the same trends in spatial metrics as those found here along an aridity gradient.](#)

230  
231 Disentangling the mechanisms driving the self-organization and stability of drylands may require  
232 metrics grounded in empirically-proven mechanisms, such as eco-hydrological feedbacks  
233 evaluated in the field by the metric *flowlength*. The fact that bare-soil connectivity increases with  
234 aridity in the healthier group of sites, and that it does so more than in the null model (Fig. 5 C left),  
235 point towards the fact that such mechanism could include resource distribution within the  
236 ecosystem (25). The consequences of this process on ecosystem stability are thought to arise from  
237 two main eco-hydrological feedbacks of opposite signs in drylands (25). At a local (patch) scale,  
238 an increase in bare-soil connectivity leads to a redistribution of resources from bare areas to  
239 vegetation patches; this self-regulating (negative) feedback is overall stabilizing. At the ecosystem  
240 scale, bare-soil connectivity increases runoff and therefore the potential losses of resources from  
241 the ecosystem; this reinforcing (positive) feedback has been shown to be destabilizing (25). The  
242 balance between these two feedback loops determines the hydrological response of the ecosystem  
243 in terms of whether connectivity is overall stabilizing or destabilizing (25) and thus the ecosystem  
244 ability to maintain itself in a productive state, or degrade into a more barren, less productive state.  
245 In the healthier group of sites, the trends in spatial metrics found are consistent with the dominance  
246 of a stabilizing feedback: an increase in bare-soil connectivity leads to more resource redistribution  
247 from bare to vegetation areas, which leads to more vegetation patchiness (i.e., deviation from  
248 random structure) and a further increase in connectivity, which contributes to the overall higher  
249 functioning (i.e., higher soil multifunctionality) and cover of these sites compared to the degraded

250 sites. Conversely, the stabilizing feedback appears weaker in the degraded group of sites. Our  
251 findings thereby empirically support one key prediction of theoretical models, namely that resource  
252 redistribution from bare to vegetated patches, driven by bare soil connectivity, is a fundamental  
253 mechanism that determines the emergent spatial structure of arid ecosystems (14, 24, 25).

254  
255 Here, our analyses identified two alternative ways in which global drylands respond to increasing  
256 abiotic stress through self-organization: one in which the vegetation patterns are building resilience  
257 but also another in which this ability of the ecosystem is lost. In the first case, i.e., in self-organized  
258 ecosystems, spatial structure reinforces itself with increasing aridity (i.e., the deviation from a  
259 random structure increases). These changes in spatial structure, which are associated with  
260 maintaining soil multifunctionality, help to mitigate the increased stress despite a decrease in cover  
261 by allowing the ecosystem to retain enough water and maintain its overall functioning, which is  
262 consistent with the idea that spatial self-organization is a mechanism of resilience at the ecosystem  
263 scale (4). Importantly, we also found that failure to perform such changes in spatial structure, and  
264 thereby retain resources, in degraded sites leads to a loss in functioning and resilience. Our results  
265 empirically highlight the essential role of spatial patterns, and more specifically of the self-  
266 organization process, for dryland functioning and resilience.

267 It is noteworthy that if vegetation patchiness allows the maintenance of cover and functioning for a  
268 large range of aridity values, it only does so below an aridity threshold of 0.8 (Fig. 2). Indeed, there  
269 are no high cover, high soil multifunctionality sites above an aridity level of 0.8. Therefore, if aridity  
270 increases beyond that threshold in some of the sites of the healthier group, we expect them to  
271 eventually shift to the degraded group of sites, thereby losing their cover and soil multifunctionality.  
272 We expect sites to shift because there are only two (or maybe 3; see Fig. S11 in SI) groups of sites  
273 globally, meaning that there is a limited number of states for dryland ecosystems to be in. This  
274 aridity threshold of 0.8 corresponds to a known documented point at which drylands exhibit a  
275 dramatic loss of vegetation cover accompanied by a decrease in species richness as well as a  
276 change in plant leaf strategy from stress tolerance to stress avoidance (27).

277  
278 Recent studies have suggested that spatial self-organization does not only contribute to increase  
279 ecosystem resilience but can also allow them to evade tipping points (4). Interestingly, our results  
280 imply that we do not have evidence that the ecosystems studied here are evading a tipping point  
281 to desertification thanks to pattern formation (as suggested for regular vegetation patterns (4)).  
282 Indeed, the self-organization process seems to only be effective in healthier sites and up to a  
283 threshold level in aridity. It is however noteworthy that we are here comparing different ecosystems  
284 in space and not following the temporal dynamics of a given ecosystem in time, which could draw  
285 a different picture of an ecosystem response to increasing stress. Learning about whether the sites  
286 studied are approaching a tipping point or not would require temporal data, a matter for future  
287 research.

288  
289 The fact that the observed changes in spatial metrics along the aridity gradient in healthier sites  
290 are consistent with theoretical predictions is a crucial step in the development of reliable indicators  
291 of desertification in drylands. Theoretical studies have suggested for a long time that the spatial  
292 structure of vegetation patterns in drylands could be used to inform about the stress level  
293 experienced by dryland ecosystems (2, 3, 11). Patch-based and hydrological metrics inform about  
294 the ability of the ecosystem to adapt to increasing stress through self-organization (i.e., they inform  
295 about 'ecological resilience' *sensu* C.S. Holling (32)), while spatial early warnings inform about the  
296 recovery of the system after a perturbation (i.e., 'engineering resilience'). Both types of metrics  
297 provide different but complementary information about the ecosystem's ability to respond to  
298 increasing stress (Fig. S4). Finding consistent trends in spatial metrics in data and models is a  
299 significant progress, but a knowledge gap still remains before we can build reliable spatial indicators  
300 of ecosystem degradation, in particular indicators which can allow us to determine which  
301 ecosystems are more fragile than others. In particular, one of the issues is that we need to get a  
302 better understanding of how different mechanisms, e.g., due to the external pressures applied on  
303 ecosystems, can affect the spatial patterns and possibly blur the signals observed here (23, 33–  
304 36). Explicit data on land use intensity is needed to be able to address that concern.

305 By combining remote sensing, field data, and model simulations, our study contributes to  
306 building a more robust framework to assess dryland degradation status. Our findings are relevant  
307 to help identifying which drylands are more fragile, and, therefore, where efforts to preserve them  
308 and prevent their degradation should be focused on. They also highlight the need for a system-  
309 level, spatial picture of dryland vegetation, since spatial structure is both a driver of increasing  
310 resilience and an early warning indicator of future ecosystem changes. Such efforts are  
311 instrumental to avoid declines in ecosystem functioning that will reduce the delivery of essential  
312 ecosystem services, forcing dryland inhabitants (which are already vulnerable) to either migrate or  
313 change their livelihood drastically in the near future.

## 314 315 316 **Materials and Methods**

### 317 Data

318 The field data set contains vegetation and soil data from for 115 dryland ecosystems located in 13  
319 countries (the data is described in details in (21)). The sites used (Fig. 1) differ widely in their abiotic  
320 (elevation, temperature and precipitation) and biotic (vegetation type, cover and number of species)  
321 characteristics (see database in figshare: <https://figshare.com/s/3db3640a61ebc975bcda>).

322 At each site, a 30 m x 30 m plot representative of the vegetation present in that area was  
323 established in the field and plant cover was estimated using the line intercept method (see more  
324 details in (21)). Five soil cores (0-7 cm depth) were taken in areas devoid of perennial vegetation  
325 (to avoid implicit effects of vegetation cover within multifunctionality measurements) and 16  
326 variables were measured related to the carbon (C; organic C,  $\beta$ -glucosidase activity, pentoses,  
327 hexoses, aromatic compounds, and phenols), nitrogen (N; nitrate, ammonium, total N, potential N  
328 transformation rate, aminoacids and proteins) and phosphorus (P; Available P, phosphatase  
329 activity, inorganic P and total P) cycles. Variables are considered to be critical determinants of  
330 ecosystem functioning in drylands. They were used to calculate a soil multifunctionality index,  
331 multifunctionality, obtained as the average Z-score across these variables (21). High values of soil  
332 multifunctionality have been associated with more functional ecosystems (20).

333 Values of the aridity index (AI, precipitation/potential evapotranspiration) were obtained from Zomer  
334 *et al.* (37), who used the data interpolations provided by Worldclim (38). To facilitate the  
335 interpretation of the results, we calculated the aridity level of each site as  $1 - AI$  (39). Indeed, as  
336 formulated, AI decreases when aridity increases, which is not intuitive; Using  $1-AI$  instead of AI  
337 solves this issue as our proxy of aridity increases as aridity does (so higher values of this aridity  
338 level indicate drier conditions), which makes our results easier to understand.

339 For each study site, remote sensing data was obtained from ref. (20). The data consists in Google  
340 EarthTM (<https://earth.google.com/>) or VirtualEarthTM (<http://www.bing.com/maps>) images of  
341 sufficient quality to visually identify vegetation patches. For each field site, three 50 m x 50 m  
342 images were collected, one of them was centered on the 30 m x 30 m plot surveyed in the field,  
343 and the other two were located nearby, avoiding strong slopes and man-made structures like roads  
344 or buildings. Each image was transformed to identify vegetation vs bare soil pixels: A k-mean  
345 classification approach implemented in Matlab (The MathWorks Inc., MATLAB v. 7.5.0.342,  
346 R2007b) was used to partition the pixels in clusters of luminance intensity (using a monochromatic  
347 version of the image) (see ref. (20) for details). The transformed images contain information about  
348 the presence or absence of vegetation in each pixel.

349 As a surrogate of plant productivity, we used the Normalized Difference Vegetation Index (NDVI),  
350 which provides a global measure of the “greenness” of vegetation across the Earth’s landscapes  
351 and is positively linked with vegetation productivity (40). This data was retrieved from previous  
352 papers (20, 21) in which NDVI data for each plot was acquired using Landsat 5 TM and Landsat 7  
353 ETM+, at a 30 m x 30 m resolution (<https://landsat.gsfc.nasa.gov/>), i.e., at the resolution of the  
354 sampled plots. For each site, the mean annual NDVI for each year between 2000 and 2015 was  
355 calculated and then averaged for the entire period.

### 356 357 358 Characterization of the spatial structure of the vegetation

359 We computed the spatial metrics on the matrices of presence-absence of vegetation inferred from  
360 the satellite images using the R package spatialwarnings (v3.0.3) (41, 42). Self-organized systems

361 exhibit common changes in spatial structure as they approach a transition (5, 41). We calculated  
362 the generic spatial early warnings that are known to capture such changes (5, 41): spatial variance,  
363 near-neighbor correlation (*Moran's I*), and spectral density ratio (*sdr*). Spatial variance, spatial  
364 correlation, and *sdr* are expected to increase as a dynamical system approaches a transition (a  
365 "bifurcation" point) (see Fig. S6 and S7 for expected trends along a stress gradient based on model  
366 simulations) (5, 17, 43, 44). Indeed, as an ecosystem is approaching a transition, neighboring cells  
367 are expected to become more similar (5). In the results, we did not display *Moran's I* as it was highly  
368 correlated with *sdr* (correlation=0.897).

369 For spatial variance, the matrices of presence-absence of vegetation were coarse-grained using 4  
370 x 4 submatrices as explained in refs. (5, 18, 45). Note that this was not the case for spatial  
371 correlation which does not require coarse-graining. The principle of coarse-graining is that each  
372 matrix of dimension  $n \times n$  is transformed into nonoverlapping submatrices of size  $s \times s$  (with here  
373  $s=4$ ). Each submatrix is then replaced by its average to obtain a smaller 'coarse-grained matrix' of  
374 size  $c_g \times c_g$  where  $c_g=n/s$  (5).

375 For each matrix, two pixels are assumed to be part of the same vegetation patch if they are  
376 neighbors (one of the four nearest neighbors, i.e., von Neumann neighborhood). We thereby  
377 calculated the size of all the patches in a given matrix and extracted a number of 'patch-based  
378 metrics'. We fitted a truncated power law to the patch size distribution of each matrix and recorded  
379 the exponent and the cutoff of the fit. We also recorded the fraction of the image covered by the  
380 largest patch using  $\log_{10}(\text{largest patch}/\text{image size})$ , where 'image size' is the number of pixels (2,  
381 5, 20, 22).

382 We calculated *flowlength*, a metric that measures the potential hydrological connectivity of runoff-  
383 source areas (e.g., bare soil) according to the vegetation cover, its spatial structure and the  
384 topography (14). *Flowlength* is defined as the average length of all the potential runoff pathways in  
385 the plot. Thus, a higher value of *flowlength* indicates a higher hydrological connectivity of runoff  
386 source areas. *Flowlength* has been suggested to be an indicator of dryland functional status by  
387 assessing potential water and soil losses in patchy landscapes (14, 24). See SI B and Fig. S3 for  
388 additional information about *flowlength* calculations.

389 To estimate whether the spatial metrics for each plot differ from what would be expected based on  
390 the amount of cover, null expectations for the values of each of the spatial metric were obtained by  
391 reshuffling the pixels of the transformed matrices 199 times (5, 18, 41). The number 199 is  
392 estimated to be sufficient in this case because subsequent analyses only depended on the means  
393 of the null distributions created. The reshuffling process removes any spatial structure from the  
394 original data while keeping the vegetation cover fixed. The same spatial metrics were then  
395 calculated on the reshuffled matrices. Note that this works well in the model, where each pixel is  
396 assumed to be a plant, but in the images, depending on the plant species, a pixel can contain many  
397 individuals or a plant (tree) can be composed of many pixels.

398 Each of these metrics is quantified on the three matrices obtained for each field site (i.e., 345  
399 values), except for *flowlength* which could only be measured on the plot among the three that was  
400 centered on the field plot (i.e., 115 values) since the slope of the field site is required to calculate  
401 *flowlength* and that information was only available for the plots sampled in the field.

402

403 Clustering analysis: splitting sites in groups

404 Clustering analyses were performed to see whether the data set could be split in different groups  
405 of sites and, if so, in how many groups. We combined multiple clustering methods to build a  
406 consensus on the number of groups in the dataset as clustering results are sensible to the chosen  
407 method and the underlying assumptions. We started by clustering the distributions of vegetation  
408 cover and multifunctionality values in our dataset (i.e., two-dimensional clustering) using  
409 hierarchical clustering (*hclust*) based on a Euclidean distance matrix and a Ward distance, which  
410 is appropriate for globular clusters (using the stats package included in R v.4.2.0 (42)). Inspecting  
411 the resulting tree (see Fig. S11) suggested that the dataset could be well-described by either two  
412 or three groups, which was confirmed by the result of a permutation-based analysis carried out  
413 using the function *simprof* in the *clustsig* R package v1.1 (42, 46), suggesting three significant  
414 groups. We further investigated this pattern based on a Gaussian mixture approach, using the best  
415 number of clusters based on the Bayesian Information Criterion (BIC). This was done using the  
416 *mclust* R package v6.0.0 in R (42, 47). This latter approach suggested the split of the dataset into

417 two groups for all but one type of cluster shape, and in this specific case, only a small increase (<2)  
418 in BIC was found by going from two to three groups (see Fig. S11). We thus considered the  
419 consensus classification into two groups as the most relevant to characterize the distribution of  
420 cover and multifunctionality in our dataset but provide all analyses for three groups in Fig. S16-  
421 S19. We used the two groups predicted by the original hierarchical clustering (Fig. S11 in SI), but  
422 those were in very close agreement (14 sites out of 345 are classified differently, 4%) with the  
423 clustering based on the Gaussian mixture approach. We refer to these two groups of sites as  
424 'healthier' (high cover – high soil multifunctionality) and 'degraded' (low cover – low soil  
425 multifunctionality).

#### 426 Identification of potential stable states

427 We used a density-based approach to detect dominant modes, which potentially reflect alternative  
428 states of the ecosystem, along the aridity gradient evaluated (48–50). This approach is based on  
429 the relationship between the empirical distribution of a set observations of a dynamical system and  
430 its potential. Assuming the following dynamical system with a single state variable  $z$ , and dynamics  
431 defined by a potential  $U$  (i.e.,  $dU/dz = - dz/dt$ ) along with a Wiener process  $dW$

$$432 dz = -U'(z)dt + \sigma dW$$

433 where  $dW$  is a Wiener process and  $\sigma$  is the noise level, it can be shown (48–50) that there is a link  
434 between the empirical distribution of observations  $p_d$  and  $U$  as

$$435 U = \frac{-\sigma^2}{2} \log(p_d)$$

436  
437  
438  
439  $p_d$  can be directly estimated from data using kernel density estimation. The above relationship  
440 formalizes the intuition that a dynamical system will tend to spend more time fluctuating around its  
441 stable equilibria, and away from its unstable equilibria. It gives a direct way to estimate what are  
442 assumed to be stable and unstable equilibria: the local minima of the potential or stable equilibria  
443 correspond to the local maxima of the density, and the local maxima of the potential or unstable  
444 equilibria correspond the local minima of the density.

445  
446 To estimate  $p_d$  along a gradient of aridity, we used a rolling-window approach in which for each  
447 value of aridity, all observations of cover or multifunctionality are taken within a range of  $x - \text{wdw}/2$   
448 and  $x + \text{wdw}/2$ , where  $x$  is the aridity value and  $\text{wdw}$  is the window size (here  $\text{wdw} = 0.15$ ). These  
449 are used to compute the distribution  $p_d$ , and thus the hypothesized stable and unstable equilibria.  
450 Doing so for all values of aridity  $x$  provides a visualization of possible stable and unstable equilibria  
451 along the gradient and an estimation of the assumed potential. The distribution of states  $p_d$  was  
452 estimated using a gaussian kernel density estimator of width 0.3 (function density() in base R). This  
453 analysis was used for Fig. 2 A, B.

#### 454 Slope of patterns along aridity & other statistical analyses

455 For the variables for which there was no replicate per site, i.e., 115 values (meaning all the variables  
456 measured in the field and *flowlength*), comparisons among two groups were done with t-tests and  
457 comparisons among the three groups with one-way ANOVA with Bonferroni adjustments of P-  
458 values.

459  
460 For all the spatial metrics for which there are three replicates per site (because of the three images),  
461 we used linear regressions to test the trends of the spatial metrics along the aridity gradient  
462 evaluated. To do so, we used a mixed-effect linear model with the site as random effect on the  
463 intercept and with either aridity or group ('healthier' or 'degraded') as the sole fixed effect. These  
464 models were fitted using the R package lme4 v1.1-29 (42). More specifically, for the analysis of the  
465 effect of aridity on spatial metrics, for example, the linear mixed model:  $I \sim \text{Aridity} + (1 | \text{site})$  was  
466 fitted to the data for each spatial metric,  $I$ . Note that the theoretical predictions provide the expected  
467 directions of change in the spatial metrics along a stress gradient (i.e., increase or decrease). The  
468 significance of the fixed effect (either aridity or group) was tested by likelihood ratio test between  
469 the full model (with the fixed and the random effect) and a model without the fixed effect (i.e., with  
470 only the random effect).

471 The slope coefficient estimated for the fixed effect in this linear model indicates how the spatial  
472 metrics (observed or null) change along the aridity gradient (a positive slope means that the metric  
473 increases with aridity). To make the slopes easier to compare across indicators and to be  
474 represented in figures, we standardized the observed and null indicator values. We computed the  
475 mean and standard deviation of all observed and null values taken together, then subtracted this  
476 mean to both the observed and null values, and divided by the standard deviation, obtaining a  
477 standardized effect size. This yielded slopes that are within the same order of magnitude for all  
478 indicators, while still allowing the comparison of observed and null slopes for a given indicator.  
479 To obtain confidence intervals on the slope estimates (and thus test significant departure from  
480 zero), we used ordinary bootstrap in which the slope was reestimated based on 2999 resampling  
481 with replacement of the data used to carry out the fit. To determine confidence intervals using  
482 bootstrapping, we need a high number of resamples so that the tails of the resulting distribution of  
483 slopes are well-sampled; we used BOOTN=2999 based on recommendations in the literature (51).  
484 The *flowlength* metric had only one value per site, thus it did not require the use of mixed-effect  
485 modelling – for this spatial metric, we used a simple linear model but did use bootstrap to get  
486 confidence intervals on the slope.

487

#### 488 Spatial models of dryland vegetation dynamics

489 We ran simulations from two mathematical models of the spatio-temporal dynamics of vegetation  
490 in dryland ecosystems. Only the results of Model 1 are displayed in the main text, while the results  
491 of Model 2 are in SI E.

492 **Model 1** (Kéfi et al. 2007). We simulated the spatio-temporal dynamics of a dryland ecosystem  
493 using a stochastic cellular automaton model that produces spatial structure of the vegetation like  
494 the one observed in empirical data (2, 5, 13, 22–24). In this model, an ecosystem is represented  
495 by a grid of cells, each of which can be in one of three states: vegetated, empty, or degraded (2).  
496 Empty cells represent fertile soil, whereas degraded cells represented eroded soil locations that  
497 are unsuitable for recolonization by vegetation. A key ecological mechanism is local facilitation, i.e.,  
498 the positive effect of vegetation on its local neighborhood through increased regeneration of  
499 degraded cells. Because of this local facilitation, vegetated cells tend to form patches, i.e., sets of  
500 vegetated cells connected by a shared edge (von Neumann neighbors, i.e., the four nearest  
501 neighbors). When aridity increases, there is a point at which the vegetation dies out and the system  
502 becomes a desert through a saddle-node (or fold) bifurcation. The model exhibits bistability for a  
503 range of aridity values (parameter  $1-b$  in the model, see SI A for a detailed model description), with  
504 the coexistence of a vegetated and a desert state (13). To evaluate the effect of the facilitation  
505 mechanism on the trends in spatial metrics observed, we also ran simulations without the facilitation  
506 mechanism. A more detailed description of the model as well as the parameter values used are  
507 available in SI A.

508 **Model 2** (Scanlon et al. 2007). We checked whether the results we obtained were similar in a  
509 second model (8), which is also a cellular automaton but considers only two possible states for the  
510 cells, namely trees and empty. The probability of establishment of new trees is assumed to increase  
511 with the neighborhood tree density, where the effect of the neighborhood tree density is a weighted  
512 as a function of the distance to the focal cell. Conversely, the probability of tree mortality increases  
513 with more empty cells in the neighborhood of a given tree. The model description, parameter values  
514 are in SI A and the results in SI E, Fig. S8 and S9.

515 **Simulations of the two models.** We ran simulations on lattices of 100x100 cells. For each aridity  
516 level, we recorded the final landscape after 10000 timesteps (for which steady state in overall cover  
517 was typically reached). All spatial metrics and their corresponding null values were computed on  
518 these landscapes (transformed into matrices of presence/absence of vegetation, i.e., removing  
519 information about whether empty sites are fertile or degraded for Model 1) in exactly the same way  
520 as previously explained for the data.

521

522

#### 523 **Acknowledgments and funding sources**

524

#### **Data sharing:**

525 The code to reproduce the analyses of the paper is available on GitHub:

526 [https://github.com/skefi/spatialews\\_biocom](https://github.com/skefi/spatialews_biocom)  
527 The data is in this folder and will be put on the GitHub repository once the paper is accepted:  
528 <https://www.dropbox.com/sh/8j4y4zm9an32rlw/AACB2O3T9vZJNYtOaBShsEQa?dl=0>  
529  
530

531 **Funding:**  
532 SK was supported by the Alexander von Humboldt foundation. This research was  
533 supported by the European Research Council (ERC Grant Agreements 242658  
534 [BIOCOM] and 647038 [BIODESERT]) and Generalitat Valenciana  
535 (CIDEAGENT/2018/041). FTM acknowledges support from the University of Alicante  
536 (UADIF22-74 and VIGROB22-350) and the Spanish Ministry of Science and Innovation  
537 (PID2020-116578RB-I00). AG has received funding from the European Union’s Horizon  
538 2020 research and innovation programme under the Marie Skłodowska-Curie grant  
539 agreement no. 896159. MB acknowledges funding from Spanish Ministry of Science and  
540 Innovation through a Ramón y Cajal Fellowship (# RYC2021-031797-I). EG  
541 acknowledges support by the Generalitat Valenciana and European Social Fund grant  
542 APOSTD/2021/188.  
543  
544

## 545 **References**

- 546
- 547 1. R. Solé, S. Levin, Ecological complexity and the biosphere: the next 30 years.  
548 *Philosophical Transactions of the Royal Society B: Biological Sciences* **377**, 20210376  
549 (2022).
  - 550 2. S. Kéfi, *et al.*, Spatial vegetation patterns and imminent desertification in  
551 Mediterranean arid ecosystems. *Nature* **449**, 213–217 (2007).
  - 552 3. M. Rietkerk, S. C. Dekker, P. C. de Ruiter, J. van de Koppel, Self-Organized  
553 Patchiness and Catastrophic Shifts in Ecosystems. *Science* **305**, 1926–1929 (2004).
  - 554 4. M. Rietkerk, *et al.*, Evasion of tipping in complex systems through spatial pattern  
555 formation. *Science* **374**, eabj0359 (2021).
  - 556 5. S. Kéfi, *et al.*, Early Warning Signals of Ecological Transitions: Methods for  
557 Spatial Patterns. *PLoS ONE* **9**, e92097 (2014).
  - 558 6. J. van de Koppel, *et al.*, Experimental Evidence for Spatial Self-Organization and  
559 Its Emergent Effects in Mussel Bed Ecosystems. *Science* **322**, 739–742 (2008).
  - 560 7. M. R. Aguiar, O. E. Sala, Patch structure, dynamics and implications for the  
561 functioning of arid ecosystems. *Trends in Ecology & Evolution* **14**, 273–277 (1999).
  - 562 8. T. M. Scanlon, K. K. Caylor, S. A. Levin, I. Rodriguez-Iturbe, Positive feedbacks  
563 promote power-law clustering of Kalahari vegetation. *Nature* **449**, 209–212 (2007).
  - 564 9. N. Barbier, P. Couteron, J. Lejoly, V. Deblauwe, O. Lejeune, Self-organized  
565 vegetation patterning as a fingerprint of climate and human impact on semi-arid  
566 ecosystems. *Journal of Ecology* **94**, 537–547 (2006).
  - 567 10. V. Deblauwe, N. Barbier, P. Couteron, O. Lejeune, J. Bogaert, The global  
568 biogeography of semi-arid periodic vegetation patterns. *Global Ecology and*  
569 *Biogeography* **17**, 715–723 (2008).
  - 570 11. J. von Hardenberg, E. Meron, M. Shachak, Y. Zarmi, Diversity of Vegetation  
571 Patterns and Desertification. *Phys. Rev. Lett.* **87**, 198101 (2001).
  - 572 12. C. A. Klausmeier, Regular and Irregular Patterns in Semiarid Vegetation. *Science*  
573 **284**, 1826–1828 (1999).

- 574 13. S. Kéfi, M. Rietkerk, M. van Baalen, M. Loreau, Local facilitation, bistability and  
575 transitions in arid ecosystems. *Theoretical Population Biology* **71**, 367–379 (2007).
- 576 14. Á. G. Mayor, S. Bautista, E. E. Small, M. Dixon, J. Bellot, Measurement of the  
577 connectivity of runoff source areas as determined by vegetation pattern and topography:  
578 A tool for assessing potential water and soil losses in drylands - Mayor - 2008 - Water  
579 Resources Research - Wiley Online Library. *Water Resources Research* **44** (2008).
- 580 15. C. Wissel, A universal law of the characteristic return time near thresholds.  
581 *Oecologia* **65**, 101–107 (1984).
- 582 16. L. Dai, K. S. Korolev, J. Gore, Slower recovery in space before collapse of  
583 connected populations. *Nature* **496**, 355–358 (2013).
- 584 17. M. Scheffer, *et al.*, Early-warning signals for critical transitions. *Nature* **461**, 53–  
585 59 (2009).
- 586 18. S. Eby, *et al.*, Alternative stable states and spatial indicators of critical slowing  
587 down along a spatial gradient in a savanna ecosystem. *Global Ecology and Biogeography*  
588 **26**, 638–649 (2017).
- 589 19. L. Rindi, M. Dal Bello, L. Benedetti-Cecchi, Experimental evidence of spatial  
590 signatures of approaching regime shifts in macroalgal canopies. *Ecology* **99**, 1709–1715  
591 (2018).
- 592 20. M. Berdugo, S. Kéfi, S. Soliveres, F. T. Maestre, Plant spatial patterns identify  
593 alternative ecosystem multifunctionality states in global drylands. *Nature Ecology &*  
594 *Evolution* **1**, 0003 (2017).
- 595 21. F. T. Maestre, *et al.*, Plant Species Richness and Ecosystem Multifunctionality in  
596 Global Drylands. *Science* **335**, 214 (2012).
- 597 22. S. Kéfi, *et al.*, Robust scaling in ecosystems and the meltdown of patch size  
598 distributions before extinction. *Ecology Letters* **14**, 29–35 (2011).
- 599 23. F. D. Schneider, S. Kéfi, Spatially heterogeneous pressure raises risk of  
600 catastrophic shifts. *Theor Ecol* **9**, 207–217 (2016).
- 601 24. Á. G. Mayor, *et al.*, Feedbacks between vegetation pattern and resource loss  
602 dramatically decrease ecosystem resilience and restoration potential in a simple dryland  
603 model. *Landscape Ecol* **28**, 931–942 (2013).
- 604 25. A. G. Mayor, S. Bautista, F. Rodriguez, S. Kéfi, Connectivity-Mediated  
605 Ecohydrological Feedbacks and Regime Shifts in Drylands. *Ecosystems* **22**, 1497–1511  
606 (2019).
- 607 26. I. Rodriguez-Iturbe, Z. Chen, A. C. Staver, S. A. Levin, Tree clusters in savannas  
608 result from islands of soil moisture. *Proceedings of the National Academy of Sciences*  
609 **116**, 6679–6683 (2019).
- 610 27. M. Berdugo, *et al.*, Global ecosystem thresholds driven by aridity. *Science* **367**,  
611 787–790 (2020).
- 612 28. J. M. Yeomans, J. M. Yeomans, *Statistical Mechanics of Phase Transitions*  
613 (Oxford University Press, 1992).
- 614 29. Ignacio Rodríguez-Iturbe, A. Rinaldo, *Fractal River Basins / Hydrology,*  
615 *hydrogeology and water resources* (Cambridge University Press, 2001) (August 16,  
616 2023).
- 617 30. O. Artime, M. De Domenico, From the origin of life to pandemics: emergent  
618 phenomena in complex systems. *Philosophical Transactions of the Royal Society A:*  
619 *Mathematical, Physical and Engineering Sciences* **380**, 20200410 (2022).

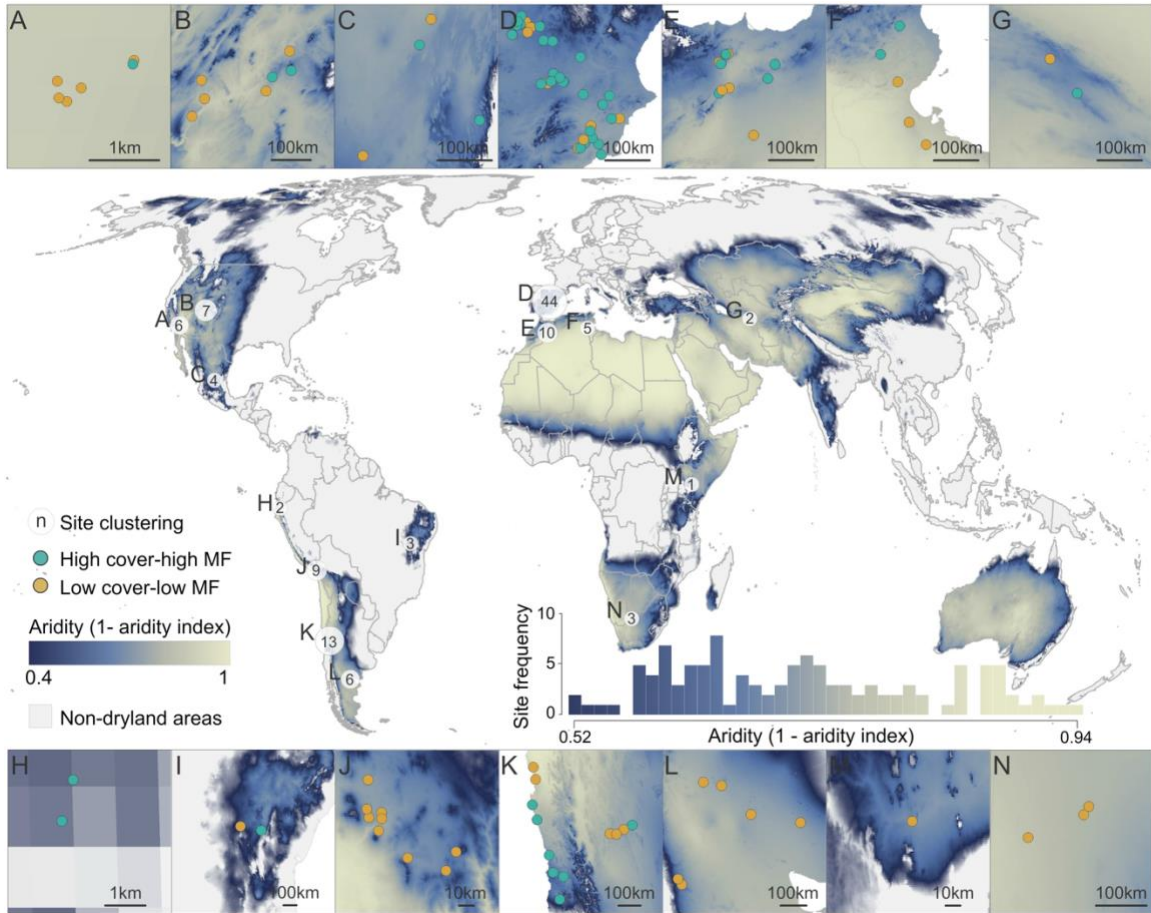
- 620 31. A. C. Staver, G. P. Asner, I. Rodriguez-Iturbe, S. A. Levin, I. P. J. Smit, Spatial  
621 patterning among savanna trees in high-resolution, spatially extensive data. *Proceedings*  
622 *of the National Academy of Sciences* **116**, 10681–10685 (2019).
- 623 32. C. S. Holling, Resilience and Stability of Ecological Systems. *Annual Review of*  
624 *Ecology and Systematics* **4**, 1–23 (1973).
- 625 33. S. Sankaran, S. Majumder, A. Viswanathan, V. Guttal, Clustering and  
626 correlations: Inferring resilience from spatial patterns in ecosystems. *Methods Ecol Evol*  
627 **10**, 2079–2089 (2019).
- 628 34. G. R. Oñatibia, L. Boyero, M. R. Aguiar, Regional productivity mediates the  
629 effects of grazing disturbance on plant cover and patch-size distribution in arid and semi-  
630 arid communities. *Oikos* **127**, 1205–1215 (2018).
- 631 35. A. Génin, *et al.*, Spatially heterogeneous stressors can alter the performance of  
632 indicators of regime shifts. *Ecological Indicators* **94**, 520–533 (2018).
- 633 36. C. Boettiger, A. Hastings, From patterns to predictions. *Nature* **493**, 157–158  
634 (2013).
- 635 37. R. Zomer, A. Trabucco, O. van Straaten, D. Bossio, “Carbon, land and water: a  
636 global analysis of the hydrologic dimensions of climate change mitigation through  
637 afforestation / reforestation” (International Water Management Institute, 2006) (October  
638 4, 2020).
- 639 38. R. J. Hijmans, S. E. Cameron, J. L. Parra, P. G. Jones, A. Jarvis, Very high  
640 resolution interpolated climate surfaces for global land areas. *International Journal of*  
641 *Climatology* **25**, 1965–1978 (2005).
- 642 39. M. Delgado-Baquerizo, *et al.*, Decoupling of soil nutrient cycles as a function of  
643 aridity in global drylands. *Nature* **502**, 672–676 (2013).
- 644 40. C. J. Tucker, C. Vanpraet, E. Boerwinkel, A. Gaston, Satellite remote sensing of  
645 total dry matter production in the Senegalese Sahel. *Remote Sensing of Environment* **13**,  
646 461–474 (1983).
- 647 41. A. Génin, *et al.*, Monitoring ecosystem degradation using spatial data and the R  
648 package spatialwarnings. *Methods in Ecology and Evolution* **9**, 2067–2075 (2018).
- 649 42. R Core Team, R: A language and environment for statistical computing. R  
650 Foundation for Statistical Computing, Vienna, Austria. (2022).
- 651 43. V. Guttal, C. Jayaprakash, Spatial variance and spatial skewness: leading  
652 indicators of regime shifts in spatial ecological systems. *Theoretical Ecology* **2**, 3–12  
653 (2009).
- 654 44. V. Dakos, E. H. van Nes, R. Donangelo, H. Fort, M. Scheffer, Spatial correlation  
655 as leading indicator of catastrophic shifts. *Theor Ecol* **3**, 163–174 (2010).
- 656 45. S. Sankaran, S. Majumder, S. Kéfi, V. Guttal, Implications of being discrete and  
657 spatial for detecting early warning signals of regime shifts. *Ecological Indicators* **94**,  
658 503–511 (2018).
- 659 46. K. R. Clarke, P. J. Somerfield, R. N. Gorley, Testing of null hypotheses in  
660 exploratory community analyses: similarity profiles and biota-environment linkage.  
661 *Journal of Experimental Marine Biology and Ecology* **366**, 56–69 (2008).
- 662 47. L. Scrucca, M. Fop, T. B. Murphy, A. E. Raftery, mclust 5: Clustering,  
663 Classification and Density Estimation Using Gaussian Finite Mixture Models. *R J* **8**,  
664 289–317 (2016).
- 665 48. M. Hirota, M. Holmgren, E. H. Van Nes, M. Scheffer, Global Resilience of

666 Tropical Forest and Savanna to Critical Transitions. *Science* **334**, 232–235 (2011).  
667 49. M. Scheffer, M. Hirota, M. Holmgren, E. H. Van Nes, F. S. Chapin, Thresholds  
668 for boreal biome transitions. *Proceedings of the National Academy of Sciences* **109**,  
669 21384–21389 (2012).  
670 50. V. N. Livina, F. Kwasniok, T. M. Lenton, Potential analysis reveals changing  
671 number of climate states during the last 60 kyr. *Climate of the Past* **6**, 77–82 (2010).  
672 51. T. J. DiCiccio, B. Efron, Bootstrap Confidence Intervals. *Statistical Science* **11**,  
673 189–228 (1996).  
674  
675  
676

677  
678  
679  
680  
681  
682  
683  
684

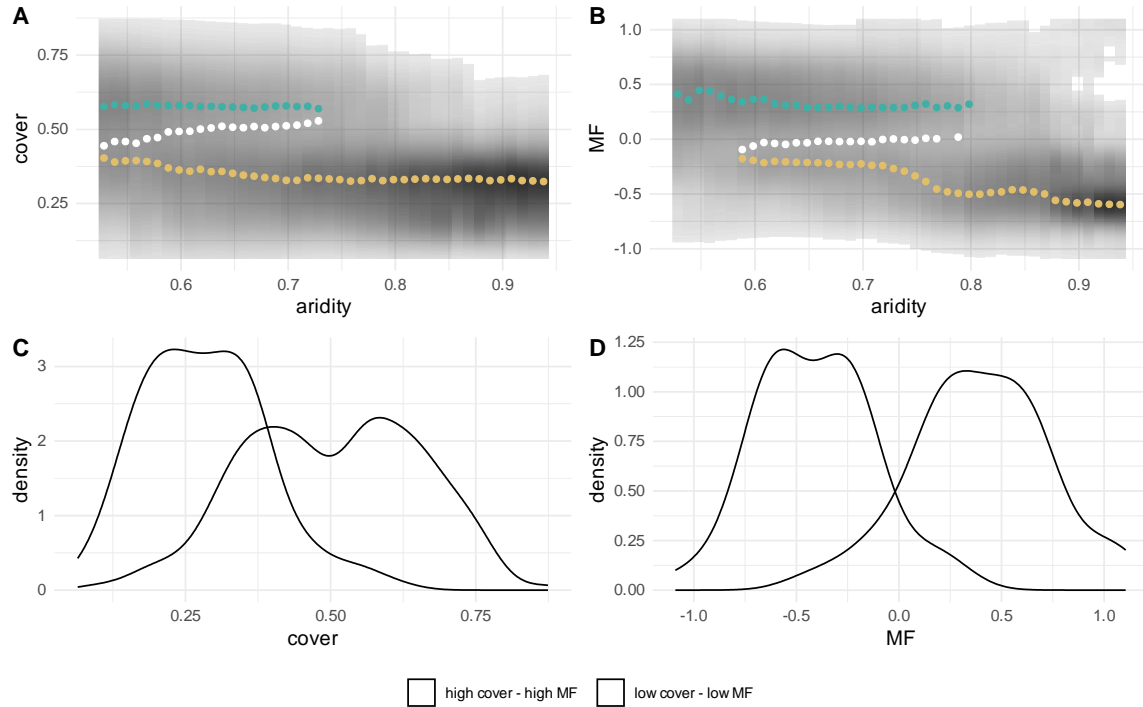
### Figure legends

**Figure 1. Location of the 115 plots in the global drylands data set used.** Surveyed sites are colored in green for the healthier sites (high vegetation cover - high soil multifunctionality, MF) and yellow for the degraded sites (low vegetation cover - low multifunctionality, MF). Numbers reflect the number of sites in a given geographical area (characterized by the letters A-N), for which a corresponding zoom can be found in the panels above and below the map.



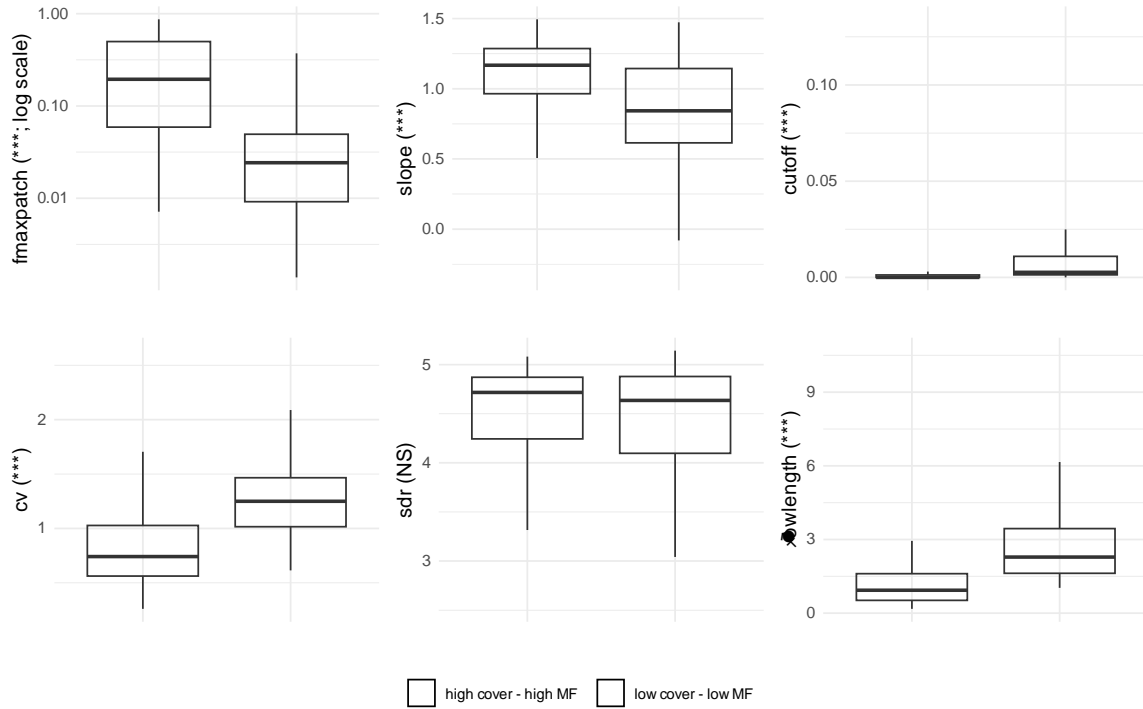
685  
686  
687  
688

689 **Figure 2. Dryland ecosystems were categorized into two groups using vegetation cover and**  
 690 **soil multifunctionality data. (A)** Cover and **(B)** soil multifunctionality (MF) along aridity for all 115  
 691 sites colored by the two groups: healthier (high cover-high soil multifunctionality values; in green)  
 692 and degraded (low cover-low soil multifunctionality values; in yellow). Aridity was calculated as:  $1 -$   
 693  $\text{Aridity Index (AI} = \text{precipitation/potential evapotranspiration)}$ , so that higher values indicate drier  
 694 conditions. Colored points are the maxima of reconstructed stability landscapes based on potential  
 695 analysis (i.e., possible attractors), while the white ones are the minima (see Materials and  
 696 Methods). Small panels below **A** display examples of stability landscapes for aridity values 0.55,  
 697 0.7 and 0.85, where valleys in the landscape are the colored points of panel A and the hills the  
 698 white points (see Materials and Methods). **(C and D)** Densities of sites for each of the two groups  
 699 for cover **(C)** and soil multifunctionality data **(D)**.  
 700



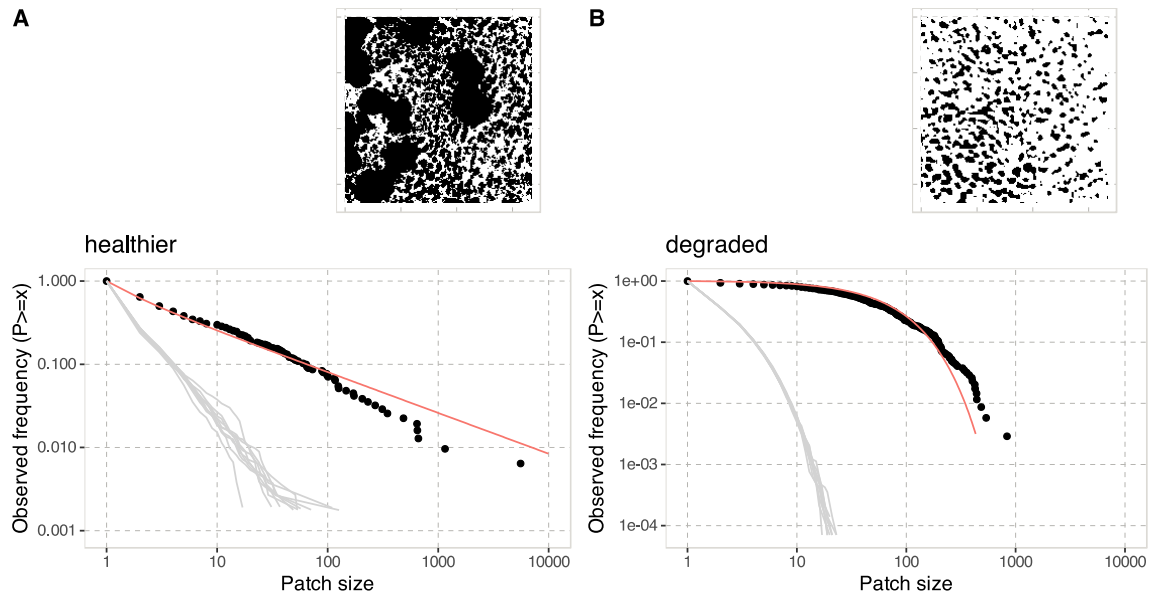
701  
 702  
 703

704 **Figure 3. Differences in the spatial structure of the vegetation cover between healthier (high**  
 705 **cover - high soil multifunctionality) and degraded (low cover - low soil multifunctionality)**  
 706 **drylands.** The spatial metrics are the proportion of the image covered by the largest vegetation  
 707 patch (*fmaxpatch*, (largest patch/image size), with the y axis on a log scale), the slope of the patch  
 708 size distribution, the cutoff of the patch size distribution, spatial variance, the Spatial Density Ratio  
 709 (*sdr*), and the bare soil connectivity (*flowlength*). For all metrics but *sdr*, the differences between  
 710 the two groups are significant (Table S3 in SI).  
 711



712  
 713  
 714

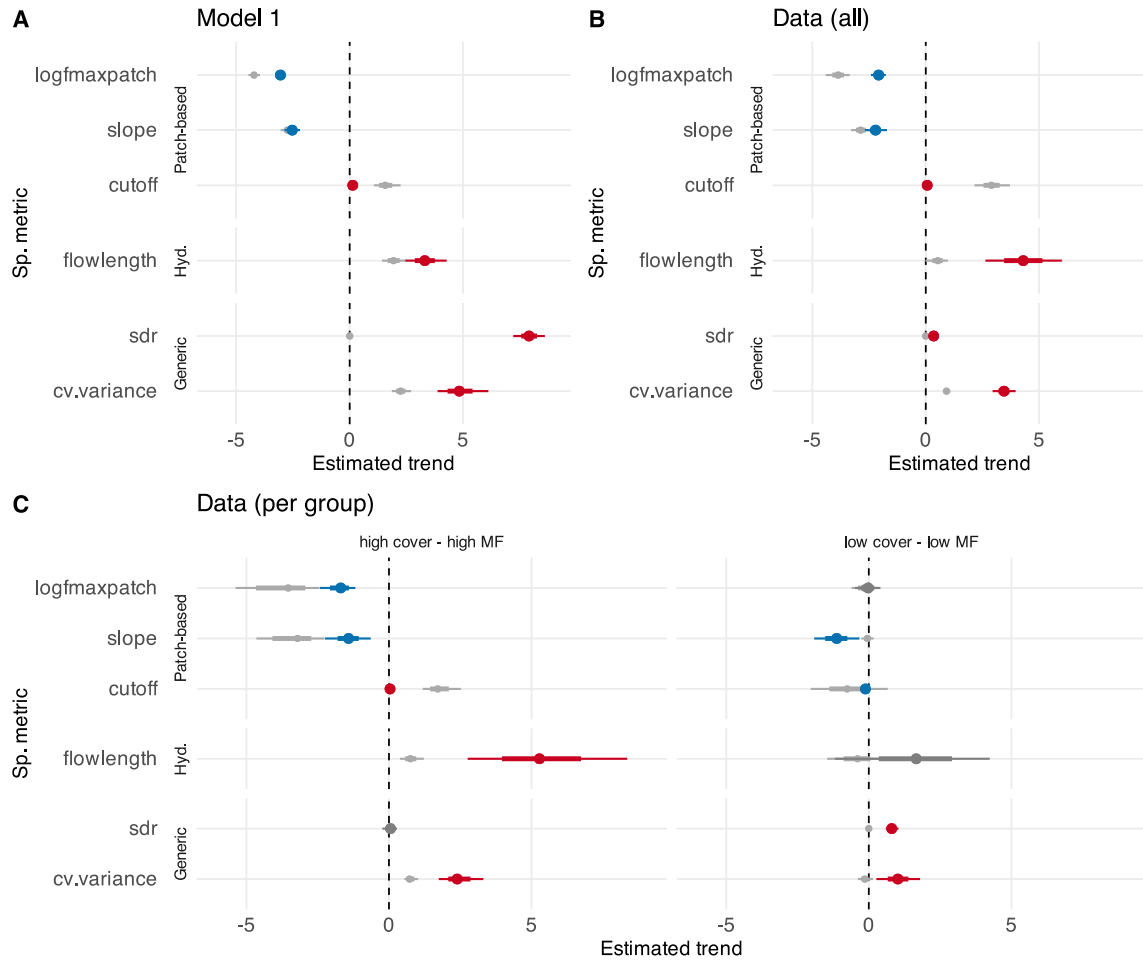
715 **Figure 4: Examples of patch size distributions of a healthier site (A) and a degraded one**  
 716 **(B).** Sites are two grasslands (images 148-b and 192-c of the data set). Graphs display the  
 717 fraction of patches larger than a certain size. Black points are observations from the image and  
 718 grey curves are random expectations (based on 10 randomizations of the image). The red curve  
 719 is the best fit. Snapshots on the top right are the images (black reflects vegetation).  
 720



721  
 722  
 723

724  
725  
726  
727  
728  
729  
730  
731  
732

**Figure 5. Estimated slope of the trends in spatial metrics along the aridity gradient evaluated in the model (A), in all the field sites of the data set (B) and in the two groups of sites separately (C; healthier sites on the left and degraded sites on the right; MF stands for soil multifunctionality).** Points reflect the value of the slope of the spatial metrics with aridity. Significant positive and negative slopes are in red and blue, respectively. Observed slopes are in color, while expected trends of randomized landscapes (keeping cover constant but with reshuffled image pixels) are in grey. See legend of Fig. 3 and Materials and Methods for definitions of the spatial metrics. See SI D for a discussion of the difference in the slopes of SDR in the model and in the data.



733